A numerical approach to design dual-scale porosity composite reinforcements with enhanced permeability

Elena Syerko, Christophe Binetruy, Sébastien Comas-Cardona, Adrien Leygue

Materials and Design 131 (2017) 307–322

Contents lists available at ScienceDirect

Materials and Design

journal homepage: www.elsevier.com/locate/matdes

A numerical approach to design dual-scale porosity composite reinforcements with enhanced permeability

Elena Syerko*, Christophe Binetruy, Sébastien Comas-Cardona, Adrien Leygue

Research Institute in Civil Engineering and Mechanics (GeM), UMR CNRS 6183, École Centrale de Nantes, 1 rue de la Noë, BP 92101, Nantes Cedex 3 44321, France

HIGHLIGHTS

- Principles for the design of multi-scale material with enhanced permeability are proposed.
- A scale separation criterion for in-plane flow through multi-scale structure is established.
- Effects of micro- and meso-scale architecture on macro-permeability are estimated.
- Differences in key geometrical parameters affecting in-plane and through-thickness flow are highlighted.
- Design of quasi-unidirectional non-crimp fabrics using established rules is presented.

GRAPHICAL ABSTRACT

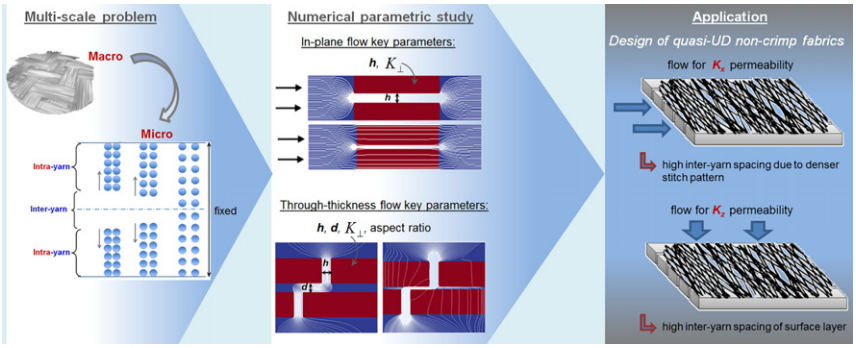

ARTICLE INFO

Article history:
Received 5 April 2017
Received in revised form 12 June 2017
Accepted 13 June 2017
Available online 15 June 2017

Keywords:
Enhanced permeability
Design
Fibrous reinforcement
Multi-scale structure
Brinkman equation
Proper Generalized Decomposition

ABSTRACT

Fibrous composite reinforcements with enhanced permeability are of a particular interest for liquid composite molding processes requiring the fibrous preforms to be well impregnated by a viscous polymer. The aim of this work is to study the link between the reinforcement permeability and the geometrical parameters of its architecture, taking into account the internal multi-scale porosity distribution by employing the Brinkman equation. In order to design a reinforcement with the enhanced permeability without degrading mechanical properties of a final composite part, the study is conducted with the condition of fixed and high fiber volume fraction. The Proper Generalized Decomposition method, due to its principle of separation of variables, allowed to efficiently compute the solution of the problem for a range of geometrical parameters at once, as opposed to the classical parametric study. A scale separation criterion for in-plane flow was proposed. It estimates when the microscopic intra-yarn flow can be neglected compared to the mesoscopic inter-yarn flow. The major contributing parameters to the enhancement of both the in-plane and through-thickness permeabilities were identified. Principles established in this study were applied to the design of quasi-unidirectional non-crimp fabrics, where the permeability enhancement was evidenced.

1. Introduction

Fabrics used as reinforcement in structural composites are usually made of woven or stitched fiber tows. Fiber tows can be viewed as clusters of fibers, and pores between tows – as tortuous channels between them. As a consequence, fabrics are a dual-scale porous medium (two-phase fibrous medium), i.e. the porosity structure composed of mesoscopic pores between fiber tows and microscopic pores between fibers inside each tow. The meso-pores offer lower flow resistance compared to the fiber tow with higher flow resistance. It is worth noting that meso-channels are always connected to micro-channels, meaning that there is no dead-end for the fluid. The

* Corresponding author.
E-mail address: elena.syerko@ec-nantes.fr (E. Syerko).

http://dx.doi.org/10.1016/j.matdes.2017.06.035
0264-1275/

ability of the fibrous medium to transmit fluid is a crucial property for Liquid Composite Molding (LCM) processes that involve infiltration of a dry fibrous preform with a liquid polymeric resin under low pressure. This family of composite manufacturing processes encompasses, among others, the Resin Transfer Molding (RTM) and Liquid Resin Infusion (LRI) processes.

The RTM process became a popular process for production of composite parts at low to medium volumes. Recent attention has focused on its development for high volume applications such as the automotive industry [1]. New low viscosity thermoplastic polymers have recently emerged to be used in technologies where long distance flow in fibrous reinforcements is the dominant mechanism. The aim is to shorten cycle times and to benefit from the advantage of thermoplastic composites in load-bearing components. High-performance composites usually require a high volume content of fibers to achieve the required mechanical properties. Then the fibrous preform contains a low volume fraction of pore space and, therefore, has a low permeability.

Although the RTM process is well adapted to low volume production, the increased volumes requested by the automotive industry introduce new constraints upon the process which are not met by current technology or by fibrous materials. The requirements of the fibrous preform for the high-speed RTM process are numerous and complex. The primary function is to reach the desired level of mechanical properties in the final part. This is achieved by designing and manufacturing a dry fibrous preform which has the suitable fiber content and orientations. The second specification is to allow fast impregnation with the lowest pressure. This has a direct influence on the cycle time and tooling cost. The third need concerns the drapability of fabrics that must allow complex shape preforms.

In the LRI process resin is drawn by the vacuum applied in the mold cavity and uses a vacuum bag to seal the fiber preform instead of a top rigid mold. As a result in this process, the thickness of the preform, and thus its permeability, change as a function of the resin pressure in the mold. In addition, the maximum pressure with which one can pull the resin into the mold is one atmosphere, leading to long fill time for large parts. Then a very porous fabric, called distribution medium, is placed on top of the fibrous medium. Since it has a very low resistance to resin flow, resin impregnates this top layer quickly and then flows into the reinforcing fibrous preform in the thickness direction. The flow in the thickness direction dramatically reduces the fill time. Contrary to the RTM process, the through-thickness permeability of the fibrous preform becomes a crucial parameter of the LRI process. Furthermore, the preform permeability has to be determined and enhanced for a wide range of fiber volume fractions.

Pearce et al. in [2,3] investigated woven fabrics, in which the architecture of the reinforcement was designed to cluster the fibers within the spiral-bound twisted tows giving consequently higher permeabilities than those of the conventional fabrics. Due to their clustered form, these flow-enhancing tows created large pore spaces next to their position. The permeability of the fabrics containing different proportions of flow-enhancing tows has been shown not to be directly proportional to the quantity of the introduced modified tows. Besides, it was found that the compression and the apparent interlaminar shear strengths decrease with an increase in the proportion of flow-enhancing tows. The authors thus concluded that the requirements of rapid processing and optimum mechanical properties are potentially in conflict, and further work is necessary to determine the best trade-off. These results suggest that a reasoning based on the overall pore space is not enough to optimize the permeability-mechanical performance trade-off.

Experimental estimation of properties of fibrous preforms for the manufacturing of composite parts by RTM still requires numerous costly tests and the identification of multiple different behaviors. The estimation of these properties by the theoretical approach is difficult due to the significant computational time required because of the multi-scale fibrous structure and the necessity to address different but strongly coupled physics. Once the problem of preform manufacturing is considered within the framework of the mechanical performance of a final composite part, other challenges are added to the aforementioned ones. As previously explained, the expectations for the fibrous preform is to have a high permeability, sufficient drapability, and to provide good mechanical properties of the final structural parts. Since high permeability and good mechanical properties are somehow in conflict, this study focuses on the first aspect with the aim to propose a reinforcement architecture with the highest permeability for a given fiber volume fraction. Then the parameter to optimize is the bidisperse porosity structure of the reinforcement in such way that the fluid can flow at both scales to minimize its dissipated power in the porous domain.

Since the fibrous reinforcements are multi-scale materials, the Brinkman equation [4,5] is employed to take into account the flow through the meso-pores (in-between the yarns), as well as the flow through the micro-pores (in-between the fibers within the yarns) for any separation of scales. It reads:

$$\phi \nabla \langle P \rangle^f = \mu \nabla^2 \langle \mathbf{v} \rangle - \phi \mu \mathbf{K}^{-1} \cdot \langle \mathbf{v} \rangle , \tag{1}$$

where $\langle \mathbf{v} \rangle$ is the fluid volume averaged velocity equal to the product of the intrinsic phase averaged velocity $\langle \mathbf{v} \rangle^f$ and porosity ϕ: $\langle \mathbf{v} \rangle = \phi \langle \mathbf{v} \rangle^f$; μ is the dynamic fluid viscosity; $\langle P \rangle^f$ is the intrinsic phase averaged pressure; $\mathbf{K}$ is the local permeability tensor of the yarn domain that characterizes the intra-yarn flow. In the majority of known studies the multi-scale effects are neglected with the application of the Darcy's law that predicts only the volume-averaged velocity, and not its local variations:

$$\langle \mathbf{v} \rangle = -\frac{\mathbf{K}}{\mu} \nabla \langle P \rangle \tag{2}$$

Attempts were also made in the literature to address the flow through the dual-scale porosity material with the help of the so-called *two-domain* approach [6–8] that describes the flow in the largest pores by the Navier-Stokes equations, and the flow through the local porous domain with micro-pores by Darcy's equation. Then an open question was about the coupling condition between the two domains in order to solve the system of equations. This question of the necessity to use a sort of empirical condition on the boundary [9] was solved by the employment of the Brinkman equation [4], containing the Stokes and Darcy terms, which was thus called a *single-domain* approach. Its advantage is that it ensures the continuity of velocity and stress on the boundary between two domains. Several studies employed the Brinkman equation to address the flow through the dual-scale porosity composite reinforcements in the LCM processes in order to determine their permeability [10–18]. For instance, in [10,11] the Brinkman equation was solved by the meshless lattice Boltzmann method (LBM), whose limitation is, however, that no acceleration techniques for the resulting system of equations are really available. Thus since the reinforcements often represent the degenerated domains, a regular LBM lattice leads to an extremely CPU time consuming calculation, even with a modest resolution of the lattice. Later, finite-difference method was employed in [14] to solve the Brinkman equation to identify the permeability of textile reinforcements of different configurations and different fiber content. In [17] the Brinkman flow problem was reduced to its 1D formulation and solved analytically in order to determine the in-plane permeability of the structure. The finite elements method (FEM) was used for the resolution in [12,15,16]. Its advantage is that the same effort for calculation is needed for the regular geometries as well as for the complex ones, and there is a large variability of fibrous structures. Control volume finite element method was employed

to solve the Brinkman equation in [18] together with the asymptotic homogenization technique to obtain the permeability tensor of woven reinforcements. In [13] the permeability tensor of multi-scale fibrous reinforcements is also suggested to be calculated by the homogenization approach from the flow at lower scale computed by the Brinkman equation. The difference of this approach with respect to [18] is that it is based on the principle of equality of dissipated powers at different scales, which is advantageous since only the velocity fields (without pressure) are needed to be calculated. In the listed studies the effects of different geometrical parameters of reinforcements, e.g. yarns spacing, crimp, nesting, on their permeability were analyzed, however, without correlating them with mechanical properties of final composite structures.

Consideration of the flow starting from the finest, microscopic scale may face non-negligible effects of capillary phenomena at this scale. However, it should be noted that the objective of this study concerns the macro-permeability of fibrous reinforcements and its enhancement, and the notion of permeability rigorously exists only in the saturated flow formulation. Therefore, further modeling is carried out in a steady-state formulation. Besides, capillary effects are determined by the fluid/fiber interaction. However, this study is focused on the reinforcement characteristics, without looking at the fluid properties.

The conventional determination of the optimal reinforcement structure implies a realization of series of calculations for different geometrical parameters. In order to reduce the computational time the PGD technique – Proper Generalized Decomposition [19,20] – is applied to this problem to obtain the solution for the multi-scale flow at once for the whole range of values of parameters of interest.

Thus, at first, Section 2 of the paper presents the model employed for the description of multi-scale flow through the fibrous reinforcement and evaluation of its energy loss, together with the general resolution methodology, which is validated against the analytic and numerical solutions of some test-cases from the literature. Section 3 describes the parametric study of influence of different geometrical parameters of the fibrous structure, both microscopic and mesoscopic ones, on the global permeability by, at first, isolating an effect of each of them, and then considering them coupled. Finally, based on the principles deduced from the numerical study, Section 4 illustrates their application to the design of fibrous reinforcements, namely the produced quasi-unidirectional non-crimp fabrics, with the enhanced in-plane, as well as the through-thickness permeability.

2. Solving methodology and validation

The Proper Generalized Decomposition method is used to solve the system of equations of momentum (Brinkman equation) and mass conservation, where the corresponding weak form after the integration by parts writes:

$$\int_{\Omega}\left(\phi\nabla\cdot\mathbf{v}^{*}\nabla\cdot\mathbf{v}+\lambda\mu(\nabla^{s}\mathbf{v}^{*}:\nabla^{s}\mathbf{v})+\mathbf{v}^{*}\left(\lambda\phi\mathbf{K}^{-1}\mu\mathbf{v}\right)\right)d\Omega=0, \tag{3}$$

for all test functions $\mathbf{v}^{*}$ selected in an appropriate functional space (where $\mathbf{v}=\langle\mathbf{v}\rangle$, $P=\langle P\rangle^{f}$ for the sake of simplicity of notation). $\nabla^{s}\mathbf{v}$ is a symmetric part of the velocity gradient. The penalization method is used to couple the velocity and pressure fields through the mass conservation condition: $\nabla\cdot\mathbf{v}+\lambda P=0$, where $\lambda<<1$ is a penalization factor. Thus only the velocity field needs to be resolved.

The efficiency of the PGD method is due to the separated representation of the sought solution in the form of a sum of functional products, each of which depends on one variable. Hence the three-dimensional solution of the Brinkman equation can be sought in the form:

$$\mathbf{v}(x,y,z)=\begin{pmatrix}u(x,y,z)\\ v(x,y,z)\\ \omega(x,y,z)\end{pmatrix}\approx\sum_{j=1}^{N}\begin{pmatrix}u_j(x)\cdot u_j(y)\cdot u_j(z)\\ v_j(x)\cdot v_j(y)\cdot v_j(z)\\ \omega_j(x)\cdot\omega_j(y)\cdot\omega_j(z)\end{pmatrix}, \tag{4}$$

where N is the number of modes – functional products in the sum – sufficient to satisfy the convergence criterion for the precise representation of the solution [19]. Each term of the expansion is computed in the iterative procedure by applying an alternating direction fixed point algorithm. The details of the PGD resolution procedure can be found in [19]. In case of a parametric study, when a series of calculations should be carried out for different values of parameters, the solution can be sought in the separated form with functional products depending not only on the space variables, but also on the selected variables-parameters. The efficient one-shot resolution by the PGD method for a range of structural parameters of fibrous reinforcements with the aim to find the ones with the enhanced permeability will be, consequently, used in this work.

Since the design of fibrous structure with the enhanced permeability does not necessarily require to know the macro-permeability values for each adjustment of the fibrous architecture, but more the trend about the macro-permeability evolution (increase/decrease), the evolution of the power dissipated by the flow through the fibrous structure can be used instead. In this case, the objective to enhance the macro-permeability becomes the objective to reduce the power dissipated at lower scale in the system. The numerical advantage of estimation of the dissipated power is that only the velocity field calculated at lower scale is needed for the evaluation, which is the case for the PGD calculation carried out for the velocity field in the penalized form.

Thus the evaluation of permeability, whose identification generally requires additionally the calculation of the pressure field at lower scale, differs from the evaluation of the dissipated power, which for the incompressible flow reads:

$$\wp=\left\langle 2\mu(\mathbf{D}:\mathbf{D})+\mathbf{v}^{T}(\mathbf{x})\cdot\mu\mathbf{K}^{-1}(\mathbf{x})\cdot\mathbf{v}(\mathbf{x})\right\rangle|\Omega(\mathbf{X})|, \tag{5}$$

where $\wp$ is the total dissipated power consisting of two terms, related to two contributions involved in the Brinkman equation: one from the so-called Stokes term and one from the so-called Darcy term; $\mathbf{v}(\mathbf{x})$ is the velocity in each point $\mathbf{x}=(x,y,z)$ of the mesoscopic domain $\Omega(\mathbf{X})$, connected to the macroscopic space $\mathbf{X}=(X,Y,Z)$; $\mathbf{D}$ is the strain rate tensor; $|\Omega(\mathbf{X})|$ is the volume of the entire domain $\Omega(\mathbf{X})$; $\mathbf{K}(\mathbf{x})$ is the tensor of local permeability of yarns; $\langle(\bullet)\rangle=\frac{1}{|\Omega(\mathbf{X})|}\int_{\Omega(\mathbf{X})}(\bullet)d\mathbf{x}$.

In order to validate the developed numerical methodology based on the PGD, the Brinkman flow problem was also solved by the classical finite elements (FEM) with the mixed velocity-pressure formulation using the Taylor-Hood elements, and then the solutions by both methods were compared to the ones available in the literature. The PGD and FEM solutions were obtained for the Brinkman flow between two infinite horizontal plates in the infinite channel, by half or entirely occupied by the uniform porous medium. Since the flow in such configurations with the prescribed velocity of magnitude unity at the inlet is constrained to be parallel to one axis, these problems have analytic solutions [21]. In the dimensionless formulation the walls of the channel were at a fixed distance 2 apart (y=±1), and the no-slip boundary conditions were set on them (Fig. 1). The dimensionless parameter of porous medium, equivalent to the notion of permeability, was equal to 0.01 (for the whole domain in Fig. 1a and for the bottom half of the domain in Fig. 1b). Further details on the analytical resolution of this dimensionless Brinkman problem can be found in [21]. The comparison of both PGD and FEM solutions with the analytic ones [21] gave an excellent agreement between the velocity profiles (Fig. 1), even without significant mesh refinement.

Other test cases from the literature were considered in order to compare the results and to make a primary analysis of the impact of geometry on the global permeability of the structure. One of the test cases represents the flow in the crosslike channel with impermeable boundaries except for the left boundary that is the inlet, and the

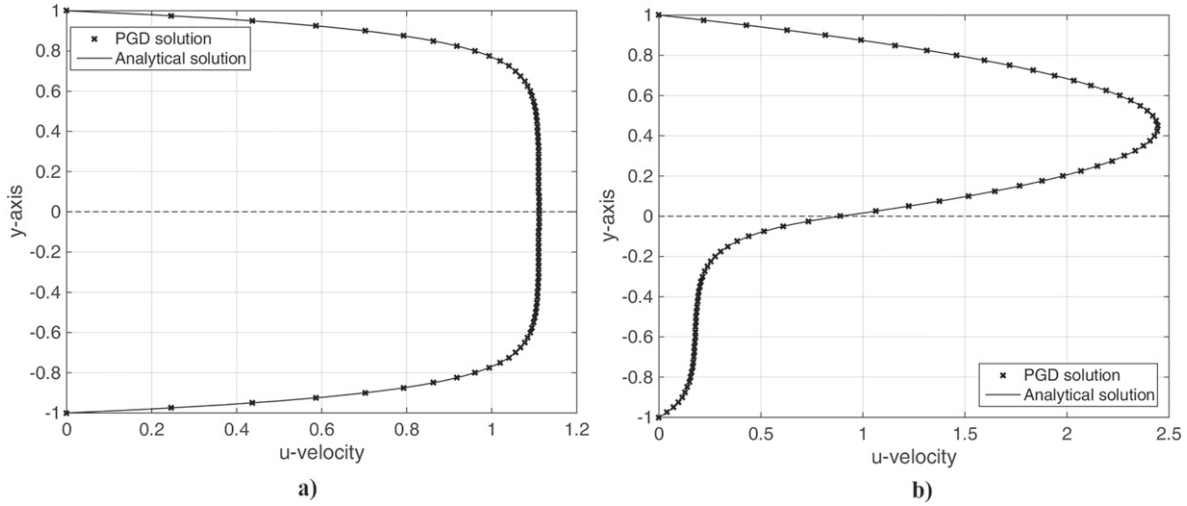

Fig. 1. Validation of the PGD solution of dimensionless Brinkman equation by comparison of obtained fluid velocity profiles with analytic solutions of: a) flow in the infinite channel entirely filled with the porous medium; b) flow in the infinite channel by half occupied by the porous medium. The dimensionless parameter of porous medium, equivalent to the notion of permeability, was set to 0.01.

right boundary that is the outlet of flow (Fig. 2), and which contains zones with different local porosities marked in gray and blue in Fig. 2. In monodisperse medium local permeability is associated monotonically with the local porosity: it increases with increasing porosity. At the inlet a parabolic velocity profile is imposed, while the no-slip boundary conditions are set on all the walls of the crosslike channel. The results of two different simulations are shown in Fig. 2a,c. The first one corresponds to the case when only the gray zones represent the porous medium Fig. 2a, where the predicted streamlines are compared to the ones reported in [21] and depicted in Fig. 2b by a solid line. Thus the flow recirculations in the vertical channel, as well as the deviated streamlines in the porous zones are obtained. It should be noted that the obtained flow recirculations should be completely symmetric, due to the geometry symmetry and the Stokes flow in the fluid zones. This is the case of the present study results, and not of [21]. In the second simulation, when compared to the first one additionally the vertical channel is also occupied by the porous medium (in gray in Fig. 2c), the flow recirculations are absent because the fluid flows through the low porosity medium. Here the predicted streamlines (Fig. 2c) are compared to the ones reported in [21] and depicted in Fig. 2b by a dotted line. Obviously, the global pressure drop of the system is higher in the second case. This fact was confirmed in this study: the problem was additionally solved by the FEM approach to obtain the pressure field.

Another test case allows to verify the effect of reducing the width of the vertical channel within the same structure (Fig. 3). This system contains the same regions of different porosity as before, the only difference being the narrowed vertical channel. The same marks are used to display and compare results in Fig. 3. Again inherent symmetrical recirculations occur in the vertical channel (however, not symmetrical in [21]) when this channel is free from porous medium. Regardless of whether the vertical channel is highly permeable or

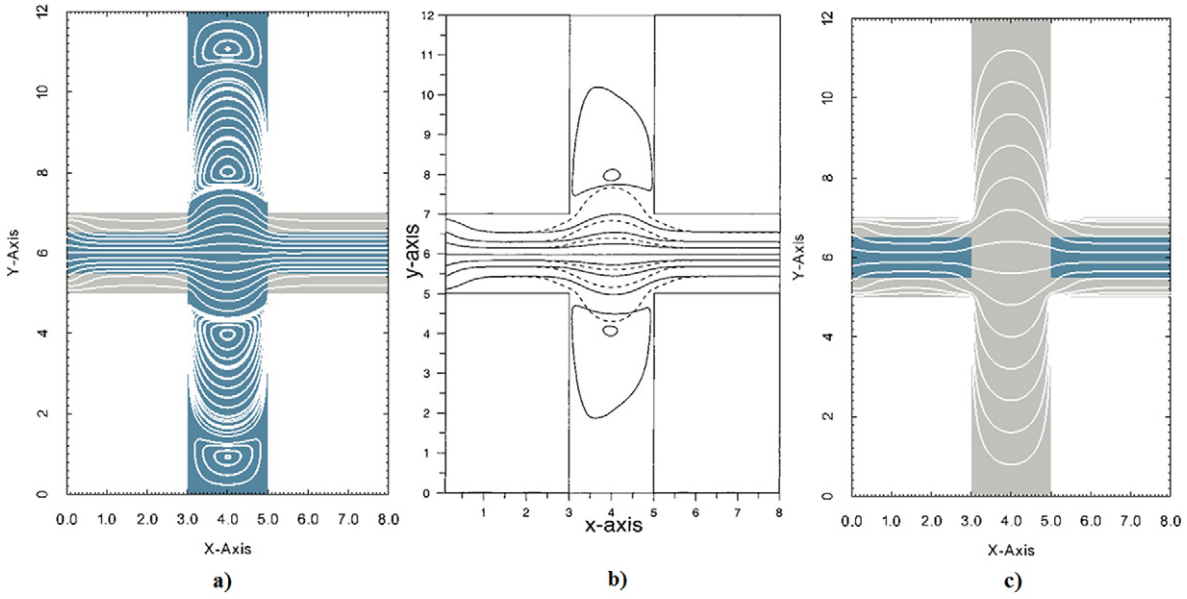

Fig. 2. Comparison of streamlines: a) results of this study: vertical channel is free from the porous medium; b) results by Al-Hadhrami et al. [21]: solid lines – vertical channel is free from the porous medium, dotted – vertical channel is low porous; c) results of this study: vertical channel is low porous. Light (gray) zones correspond to the porous medium with the dimensionless parameter 0.01, equivalent to the notion of porosity.

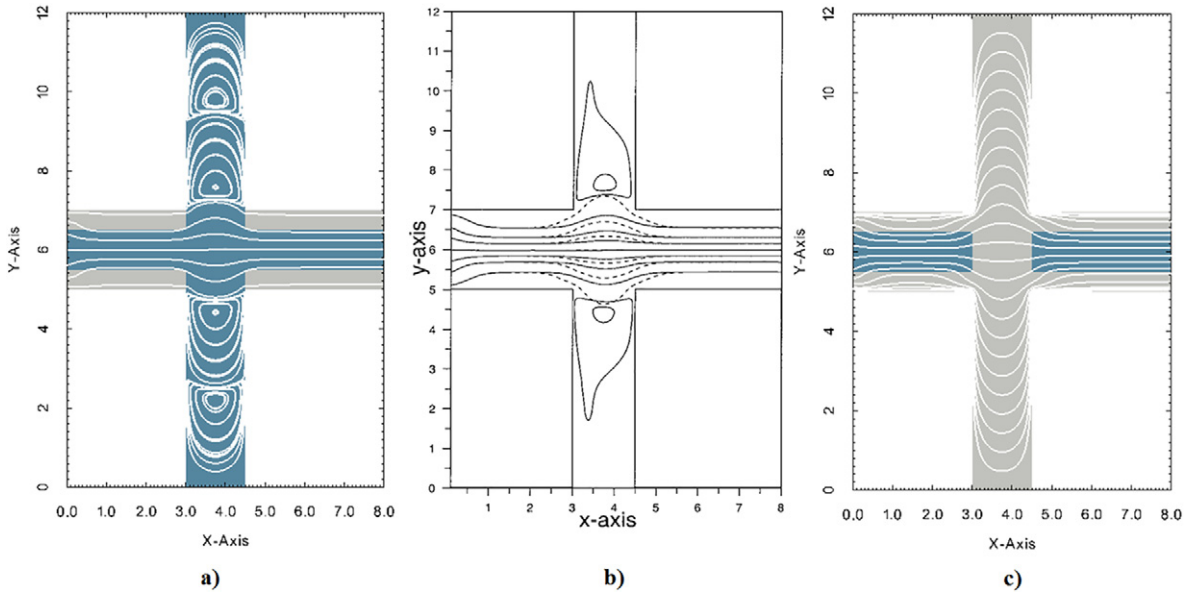

Fig. 3. Comparison of streamlines for the case of narrowed vertical channel: a) this study results: vertical channel is free from the porous medium; b) results by Al-Hadhrami et al. [21]: solid lines – vertical channel is free from the porous medium, dotted – vertical channel is low porous; c) this study results: vertical channel is low porous. Light (gray) zones correspond to the porous medium with the dimensionless parameter 0.01, equivalent to the notion of porosity.

low permeable, the magnitude of the fluid velocity in this region increases as the width of the vertical channel decreases. This is seen by the concentration of streamlines towards the axis of symmetry. As shown in [21], unlike the velocity variation along the width of the vertical channel, the overall pressure gradient changes depending on if the vertical channel is highly permeable or not. Thus the problem was also solved by the FEM to obtain the overall pressure drop (Fig. 4). Pressure fields in Fig. 4a and c correspond to the configurations in Fig. 3a and c respectively. As the vertical channel is highly permeable (Fig. 3a), narrowing of the vertical channel forces the fluid to flow more in region of low permeability within the exit channel. Thus the overall pressure gradient increases, with a percentage increase of about 5% (Fig. 4a) compared to the initial configuration with the same distribution of porosities (Fig. 4b). If the vertical channel has a low permeability (Fig. 3c), the reduction of the channel width implies that while the fluid has to pass more through the layered exit channel zone, it is at the expense of having to flow less through the flow-resistant layered vertical channel, and thus the overall pressure gradient decreases by about 10% (Fig. 4c) compared to the initial low permeable configuration, whose pressure field is depicted in Fig. 5a. The predicted pressure changes and the ones reported in [21] correlate well.

One more configuration was considered with the additional tortuosity of the flow introduced by shifting the outlet channel (Fig. 5). The distribution of local porosities was the same as in the first test case simulation and fixed. The flow streamlines calculated by the PGD and obtained in [21] are in good agreement. An increase of the pressure drop due to the displacement of the outlet channel is observed (Fig. 5). The difference between the pressure drops in the two configurations depicted in Fig. 5a,b is the more significant the lower the permeabilities of local zones are. The effect of the local flow tortuosity on the global permeability is studied in detail in the sequel.

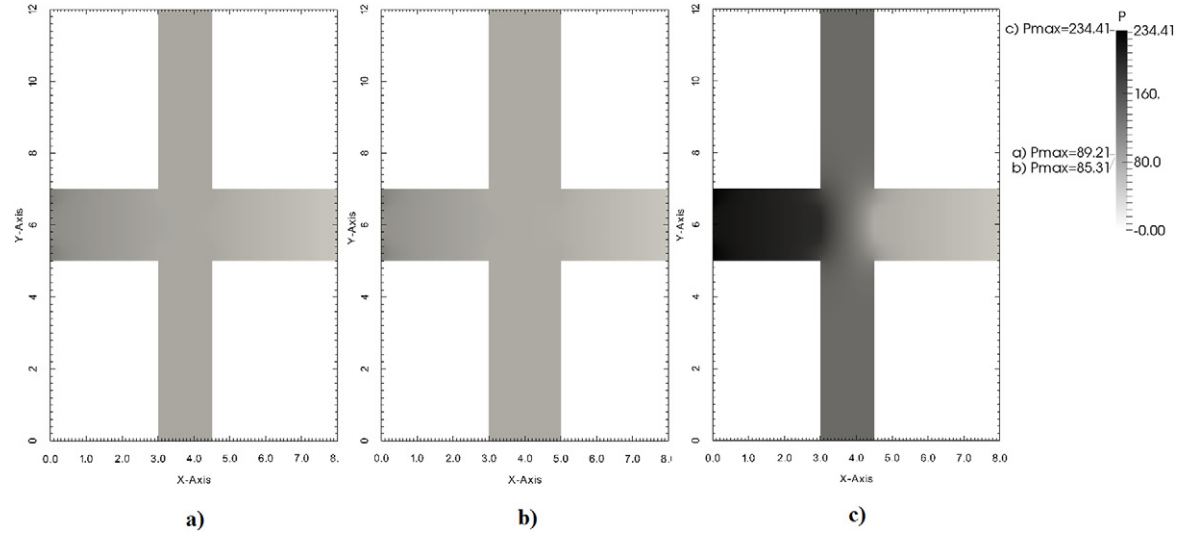

Fig. 4. Effect of reduction of the vertical channel width on the pressure field: a) vertical channel is narrowed and free from the porous medium; b) vertical channel with the initial width and free from the porous medium; c) vertical channel is narrowed and low porous.

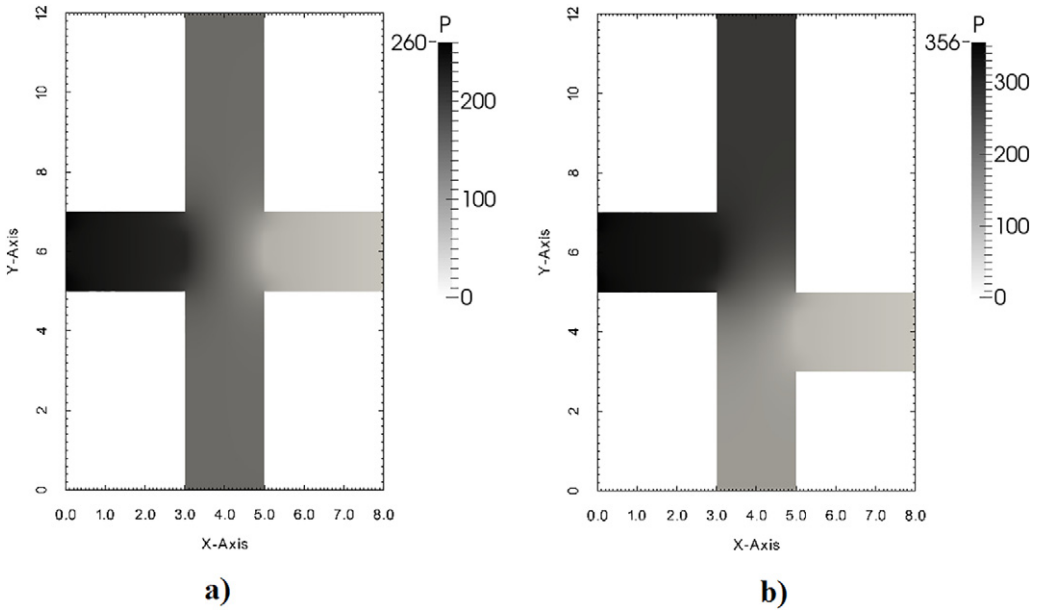

Fig. 5. Effect of the flow tortuosity on the pressure fields in the porous medium. Dimensions of regions with different porosities are the same as in Fig. 2c.

3. Influence of geometrical design parameters on permeability

3.1. Analysis of micro-/mesoscopic flow effects

The objective of this study is to design a fibrous material with an enhanced permeability taking into account its dual-scale porosity structure. Understanding the flow mechanisms at the microstructural level is clearly necessary in order to achieve this goal. This question has already been raised in the literature, for example, by Beavers and Joseph in [9], Summerscales et al. in [22]. However, attempts of correlating permeability to easily measured properties of the fibrous structure have often been unsuccessful. The most widely known relation is the Kozeny-Carman equation, which is based on a semi-empirical model of Poiseuille flow through pore channels:

$$K = \frac{1}{C_k S^2 \tau^2} \frac{(1 - V_f)^3}{V_f^2}, \tag{6}$$

where S is the specific surface, defined to be the fluid/fiber interfacial area per unit total volume, τ is the tortuosity factor, V_f is the fiber volume fraction, and C_k is the shape-dependent constant.

The Kozeny-Carman relation, being scalar rather than tensorial (i.e. isotropic rather than orientation-dependent) is unsuitable for anisotropic fibrous materials. In the absence of an available predictive model to relate the permeability of structured double-scale porosity fabrics to appropriate architectural parameters, it is of interest to analyze, at first, the influence of different geometrical parameters on the multi-scale and anisotropic nature of the flow, to check which part of the porous structure actually contributes to the flow. This is by nature a computationally expensive parametric problem. As mentioned before, the PGD method allows to efficiently compute the parametric solution by representing it in a separated form of product of functions, each of which being dependent on one variable-parameter. Thus the dimensionality of the problem is considerably reduced, as a series of 1D problems should be solved instead. This point will be explained in more detail in an example in the sequel.

For the parametric study two geometrical parameters, each representing a different scale of interest, were selected. One parameter is the characteristic size of the inter-yarn pores, which will be called *meso*-channels size h, compared to the *micro*-scale flow between the fibers inside the yarn and *macro*-scale flow through the whole part usually described by the Darcy's law. Another parameter is related to the micro-scale (scale of fibers), the typical pore size of which is often estimated as $\sqrt{k}$, where k is the local permeability inside the yarns. So the solution of the Brinkman problem is sought in the separated form dependent not only on the space coordinates, but also on extra-coordinates h, the meso-pores size, and the micro-permeability of yarns. The flow through a fibrous structure depicted in red in Fig. 6 with yarns of fixed thickness a distant from each other at varying h is considered. Here the yarns depicted in Fig. 6 are perpendicular to the macroscale flow. Thus the problem is considered in 2D-space formulation with transversally isotropic yarns. Such yarn orientation with respect to the macro-flow is initially chosen in order to begin a study with the cases of maximum micro-/macro- scales separation. The boundary conditions imposed (Fig. 6) are the parabolic velocity profile at the inlet (left boundary), and no-slip conditions at the boundaries parallel to the flow direction (top and bottom). It should be noted that without loss of generality a rectangular shape of yarns is used in the model for the question of simpler separated representation in Cartesian coordinates of the domain geometry for the application of the PGD method. The flow problem with elliptical yarns as well has been solved by the FEM for verification. Naturally, compared to the equivalent rectangular geometry of yarns, smoother geometry results in a lower dissipation of energy by the flow in such domain (i.e. a higher permeability). However, according to the objective of this study knowing separately for each case the order of magnitude of the dissipated power is not required, but the trend of its evolution with the change of parameters is of interest. Therefore, since it has been verified that the change of the selected design parameters affects the dissipated power in the domain with elliptical shapes in the same way that in the domain with idealized shapes, further study is justified to be conducted with the geometries separable in the Cartesian coordinates and by the PGD method.

The permeability $k_\perp$ of the plane of transverse isotropy of yarns with local tensor $\mathbf{K} = \begin{pmatrix} k_\perp & 0 \\ 0 & k_\perp \end{pmatrix}$ is variedindependently as the varying distance h. Hence the velocity field $\mathbf{v}$ is sought for in a separated form dependent on the space coordinates, the distance h, and the permeability $k_\perp$. It should be noted that since all coordinates in the separated representation should be independent, and for an a priori fixed space discretization the second space coordinate y becomes

Fig. 6. In-plane flow domain with varying distance h between yarns of fixed thickness a (in red) and varying local permeability. Inter-yarn pores (in blue) are crossed by streamlines (white solid lines), also actively penetrating yarns when $h = h_{min}$.

dependent on the varying inter-yarn distance h, a diffeomorphism $y(s)$ between the physical and parametric domains: $\Omega^s \rightarrow \Omega^y$ is introduced so that new PGD parametric coordinates s and h are independent from each other following the method of [20,23,24]:

$$y = \begin{cases} s & \text{if } s \in [0, a] \\ (s-a)\cdot h/h_{min} + a & \text{if } s \in (a, a + h_{min}) \\ s - h_{min} + h & \text{if } s \in [a + h_{min}, 2a + h_{min}] \end{cases} \quad (7)$$

where s is the parametric second space coordinate, h_{min} is a lower bound of the range of h chosen in the simulation – the minimal inter-yarn pore size (defined as the one approaching the intra-yarn pore size); a is the yarn dimension in s-direction. With this change of variable, Jacobian matrix owns constant-value components 1 or $\frac{h}{h_{min}}$ over each subdomain. Thus the separated form of the velocity field $\mathbf{v}$ writes:

$$\mathbf{v}(x, s, h, k_\perp) = \begin{pmatrix} u(x,s,h,k_\perp) \\ v(x,s,h,k_\perp) \end{pmatrix} \approx \sum_{j=1}^{N} \begin{pmatrix} u_j(x)\cdot u_j(s)\cdot u_j(h)\cdot u_j(k_\perp) \\ v_j(x)\cdot v_j(s)\cdot v_j(h)\cdot v_j(k_\perp) \end{pmatrix} \quad (8)$$

Then the weak form of the problem after the integration by parts writes:

$$\int_0^{x_{max}} \int_0^{s_{max}} \int_{h_{min}}^{h_{max}} (\phi \nabla\cdot\mathbf{v}^* \nabla\cdot\mathbf{v} + \lambda\mu \nabla^s\mathbf{v}^* : \nabla^s\mathbf{v} + \mathbf{v}^*\cdot\lambda\phi k_\perp^{-1}\mu\cdot\mathbf{v}) \, dx \frac{\partial y}{\partial s} ds dh = 0 \quad (9)$$

where the divergence and gradient of $\mathbf{v}$ contain the information from y-function.

The classical numerical computation would imply the resolution of the problem for each combination of values of two selected parameters, i.e. $(N_h \cdot N_k)$ of 2D problems, if N_h and N_k are the numbers of degrees of freedom (DOF) of the parameters h and $k_\perp$ respectively. While with the "on-line" particularization of the obtained one PGD "off-line" 4D solution related to different ratios between the size of inter-yarn pores and the intra-yarn permeability, different flow fields were observed and analyzed in post-processing. In this case $(4 \cdot N)$ of 1D problems were solved, with N being the number of PGD modes of the solution (8) in 4D space of variables. Therefore, the dimensionality of the problem is reduced, the discretizations $N_h > 4$, $N_k > 4$ compared to the product $(4 \cdot N)$, and the number of PGD modes N was always <40 for the problems considered in this study. If n is the average number of DOFs of each dimension, the cost of the classical FEM computation increases exponentially according to n^{dim}, where dim is the number of dimensions of the problem, equal to 4 in this case. While the cost of the PGD computation increases linearly according to $n \cdot dim \cdot N$. The higher the problem discretization needed and the higher its dimensionality, the higher the computational savings the PGD gives compared to the FEM. Another example of comparison data of the PGD and FEM computational costs for the spatially 3D problems with 2D + 1D variables separation can be found in [25].

The parametric calculation allowed to determine the condition, at which the microscopic flow inside the yarns can be neglected compared to the mesoscopic flow between the yarns. For convenience and to be coherent with the literature considerations [5,9,21], the considered correlation between the characteristic meso-pores size h and characteristic micro-pores size $\sqrt{k_\perp}$ was expressed in the form of non-dimensional ratio $k_\perp/h^2$. If this ratio between the local transverse permeability $k_\perp$ of yarns and the size h square is smaller than 10^{-3}, the flow through the fibrous structure can be simplified and can be considered as a single-scale flow: $k_\perp/h^2 < 10^{-3}$. The limiting value of the condition was found from the estimation of maximal fluid velocity in intra-yarn pores that in the case of single-scale flow should not exceed 1% of the maximal velocity in inter-yarn pores. Thus in this case the flow is dominantly guided by the meso-channels between the yarns, as will be shown in the sequel, flowing around the yarns and thus increasing the main flow tortuosity. The tortuosity is considered in this study as a flow feature induced by the reinforcement architecture and influencing its global permeability. Thus it is important to analyze it for the design of tailored reinforcements.

The multi-scale nature of flow through the fibrous reinforcement can be estimated with the help of the graph of ratio $k_\perp/h^2$ in Fig. 7 that covers the range of typical sizes of meso-pores: from 20 μm to 1 mm. Supposing that the typical fiber radii range between $[2\mu m; 10\mu m]$, and that the local volume fraction of fibers within the yarn is usually higher than 50%, the local permeability of transverse isotropy of yarns $k_\perp$ can have the order of magnitude from approximately 10^{-18} m^2 to 10^{-12} m^2. It can be calculated, for example, by the relations proposed by Gebart [26].

The information about the local fiber volume fraction of yarns is not usually available, and its evaluation needs an additional effort. Consequently, in order to estimate from Fig. 7 if the flow has a single- or multi-scale character, a range of possible local permeabilities can be evaluated by the Gebart's relations from a range of possible local V_f bounded below by the value of global V_f of the reinforcement, usually known. With the known (usually) meso-pores size the easiest visual way is to plot the vertical line corresponding to the range of evaluated permeabilities with respect to the graph in Fig. 7. If the line does not cross the graph, the scale separation is identified for this reinforcement without the knowledge of local V_f inside the yarns.

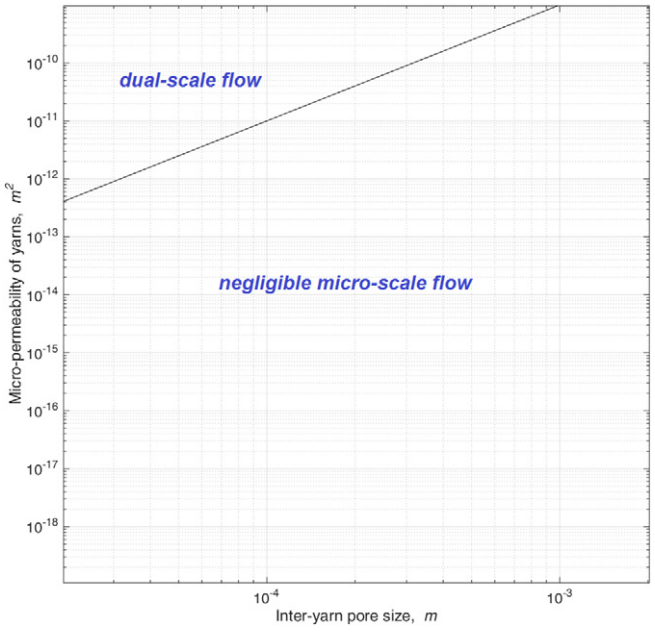

Fig. 7. In-plane flow scale separation criterion for the relation $k_\perp/h^2 \gtrless 10^{-3}$ between the tows transverse micro-permeability $k_\perp$ versus the inter-tow channel size h.

3.2. Influence of parameters of the simplified structure

The test cases considered for validation of the methodology, as well as the proposed criterion of scale separation that relates the mechanisms of micro- and mesoscopic in-plane flow, allow to deepen the analysis of different reinforcement structural configurations to propose the one with the enhanced in-plane permeability. Another feature that affects the energy dissipated by the fluid flowing through the fibrous medium, and which, therefore, may enhance (or decrease) the permeability, is the flow tortuosity induced by the complex architecture of fibrous reinforcement.

The first consideration of the possible optimal configuration consists of calculation of flow through the unidirectional structure (2 layers) with different levels of compaction of yarns, while the global fiber volume fraction is fixed with the aim to preserve mechanical properties of the resulting fiber reinforced polymer composite. The evolution of geometrical parameters values is chosen so that different flow modes with respect to the condition $k/h^2 \gtrless 10^{-3}$ could be checked: negligible or non-negligible flow at microscopic scale. The considered evolution of the fibrous architecture is schematized in Fig. 8a. To maintain the global fiber volume fraction constant, while reducing the inter-yarn pores with the fixed total thickness H, the transverse permeability of yarns, whose local V_f decreases, should change and be reestimated for each reorganization within the structure. It was done by using the relation of Gebart for quadratic packing of fibers inside the yarn [26]. Without loss of generality and for the convenience of domain separation for the PGD method, the yarns linear dimensions are changed while preserving their rectangular form.

Suppose that the multi-scale fibrous structure is changed starting from the uncompacted case where the yarns are close to each other with the distance h_{min} between them. In this example the fibers radius $r = 11\mu m$ and the distance between them ($5\mu m$ at first, Fig. 9) are defined in the way not to exceed the relation of this distance to the fiber diameter that should be much smaller than 1, in order to be able to use the Gebart relations to evaluate the local permeability of yarns. So in this case the local permeability of yarns is high enough, the streamlines penetrate the yarns (Fig. 8b bottom), and the flow tortuosity is low. On the contrary, when the inter-yarn pores grow, the yarn permeability decreases (since the global V_f is fixed by the fixed thickness H), the flow at micro-scale is now negligible: the streamlines get around the yarns, which enlarges the main flow tortuosity (Fig. 8b top).

Within the framework of parametric computation by the PGD method the described evolution of geometrical parameters means that the space coordinates of yarn domains change with the change of parameter h of meso-pores. Besides, the local permeability of yarns $k_\perp$ is not an independently changing parameter anymore (unlike the way it was considered in the previous section) because it is restricted by the fixed total V_f. Thus for the calculation of the velocity field in a separated form the following piecewise linear changes of variables are needed to make the coordinates t, s, and h to be independent:

$$y(s) = \begin{cases} s\cdot(H-h)/2, & \text{if } s \in [0,1] \\ (s-1)\cdot h + (H-h)/2, & \text{if } s \in [1,2] \\ H-(3-s)(H-h)/2, & \text{if } s \in [2,3] \end{cases} \tag{10}$$

for the coordinate s in the direction of thickness of the structure. And for the coordinate t in the in-plane direction the diffeomorphism writes:

$$x(t) = \begin{cases} t\cdot(l_x-l)/2, & \text{if } t \in [0,1] \\ (t-1)\cdot l + (l_x-l)/2, & \text{if } t \in [1,2] \\ l_x-(3-t)(l_x-l)/2, & \text{if } t \in [2,3] \end{cases} \tag{11}$$

where l_x is the size of the whole domain in t-direction, and l is the changing yarn width that should be recalculated with respect to the change of parameter h. It should be noted that depending on the domain dimensions the diffeomorphisms (10)–(11) should be multiplied by an appropriate scale factor. Then $y(s)$ and $x(t)$ should be represented in a separated form. The sought for velocity field is thus calculated in the following separated representation:

$$\mathbf{v}(t,s,h) = \begin{pmatrix} u(t,s,h) \\ v(t,s,h) \end{pmatrix} \approx \sum_{j=1}^{N} \begin{pmatrix} u_j(t)\cdot u_j(s)\cdot u_j(h) \\ v_j(t)\cdot v_j(s)\cdot v_j(h) \end{pmatrix} \tag{12}$$

For quadratic packing of fibers within the yarn the relation for the yarn dimensions evolution is $(l_1+\Delta_1)/(h_{yarn_1}+\Delta_1) = (l_2+\Delta_2)/(h_{yarn_2}+\Delta_2)$, where l can be defined from the fiber radius and number of fibers, $h_{yarn} = (H-h)/2$, Δ is the changing inter-fiber distance (Fig. 8a). Thus if the initial dimensions of yarns are known, for instance the ones corresponding to the smallest local fiber volume fraction l_{max} and $h_{yarn_{max}} = (H-h_{min})/2$, then the derivation of evolution of l gives:

$$l = \frac{-(l_{max}-2r)}{H-4r-h_{min}}h + \frac{(H-4r)l_{max}-2rh_{min}}{H-4r-h_{min}} \tag{13}$$

depending on 4 constant parameters: fixed total thickness H, fiber radius r, and two initial dimensions of yarns l_{max} and $h_{yarn_{max}} = (H-h_{min})/2$, from which the corresponding inter-yarn distance

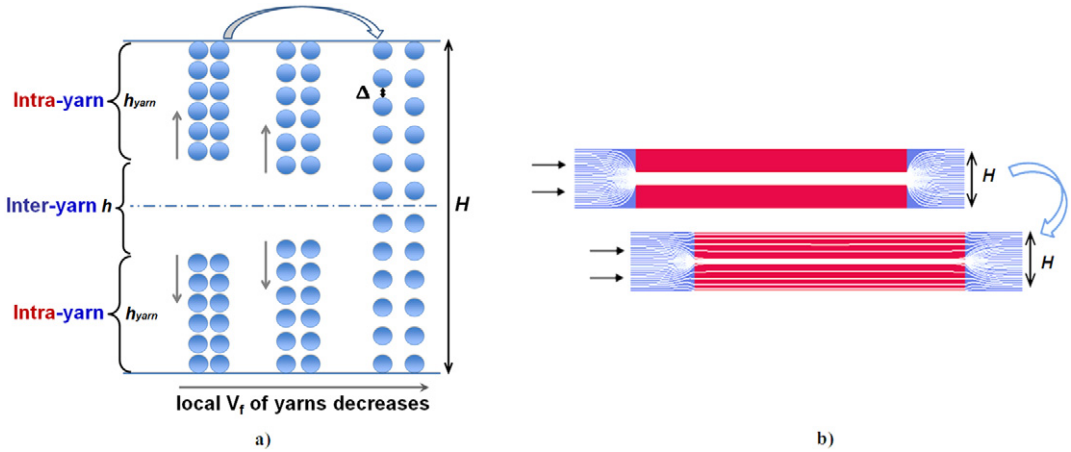

Fig. 8. In-plane flow through unidirectional reinforcement: a) increase of the local permeability and decrease of inter-yarn voids with the fixed total thickness H and V_f; b) yarns (red) and inter-yarn voids (blue) with streamlines (solid white lines): top – yarns of low permeability, bottom – yarns of high permeability.

Flow mode	Negligible at micro (high tortuosity)		Non-negligible at micro (low tortuosity)
Distance between fibers	1 μm	2.5 μm	5.5 μm
Distance between yarns	127.73 μm	97.73 μm	37.73 μm
Permeability $k_\perp$ of yarns	$2.13\cdot10^{-14}$ m^2	$2.11\cdot10^{-13}$ m^2	$1.51\cdot10^{-12}$ m^2
Macro-permeability	$2.65\cdot10^{-10}$ m^2	$1.24\cdot10^{-10}$ m^2	$1.15\cdot10^{-11}$ m^2

Fig. 9. Influence of micro- and mesoscopic parameters on the global in-plane permeability of fibrous reinforcement. Here fiber radius $r = 11\mu m$, $V_{f_{total}} = 48\%$.

h_{min} can be expressed. Thus l linearly changes with the change of parameter h.

The evolution of the transverse permeability $k_\perp$ of yarns should also be expressed as a function of inter-yarn distance h. According to [26], for quadratic packing of fibers $k_\perp = \frac{16}{9\pi\sqrt{2}}\left(\sqrt{\frac{\pi/4}{V_f}} - 1\right)^{5/2} r^2$. Therefore, V_f of the yarn should be expressed as a function of h. The expression is derived based on the geometrical reasoning that local fiber volume fraction $V_f = V_{f_{total}}/V_{f_{meso}} = V_{f_{total}}/(1-\varphi)$, where φ is the mesoscopic porosity, i.e. the relation of inter-yarn pores to the total volume of the domain. The derived expression for the local V_f reads:

$$V_f = \frac{V_{f_0}(H - h_{min})l_{max}(H - 4r - h_{min})}{(H-h)((2r - l_{max})h + (H-4r)l_{max} - 2rh_{min})} \tag{14}$$

where V_{f_0} is the local V_f corresponding to the known initial dimensions of yarns l_{max} and $h_{yarn_{max}}$.

With the derived relations the weak form of the problem writes:

$$\int_0^{t_{max}}\int_0^{s_{max}}\int_{h_{min}}^{h_{max}} (\phi\nabla\cdot\mathbf{v}^*\nabla\cdot\mathbf{v} + \lambda\mu\nabla^s\mathbf{v}^* : \nabla^s\mathbf{v} + \mathbf{v}^*\cdot\lambda\phi k_\perp^{-1}\mu\cdot\mathbf{v})\frac{\partial x}{\partial t}\frac{\partial y}{\partial s}dtdsdh = 0 \tag{15}$$

where the divergence and gradient of $\mathbf{v}$ contain also the information from x and y functions. The power dissipated in the domain is then evaluated using Eq. (5) from the velocity fields calculated in a separated form for a range of values of the parameter h. The obtained evolution of the dissipated power shows that with the change of the flow mode from predominantly mesoscopic to multi-scale it has a monotonic character, there is no extremum. It decreases with the increase of meso-pores between the yarns, which means that the macroscopic permeability increases, while the local permeability of yarns, on the contrary, decreases.

In order to know the order of magnitude of macro-permeabilities corresponding to the considered unidirectional configurations, three discrete cases for three values of the parameter h were selected and solved by the FEM as well. The data of the simulated cases are summarized in Fig. 9 and represent two situations where the flow shows a single-scale character, and one with a multi-scale character. With the pressure fields computed by the FEM approach the global permeability was then evaluated by the identification from the Darcy's law as follows: $K = \frac{Q}{A}\frac{\mu}{\nabla P}$, where Q is the imposed flow rate in the domain, A is the area of the domain cross-section exposed to the imposed flow, μ is the fluid viscosity, and ∇P is the computed pressure gradient. Analogously to the trend of the dissipated power, the macro-permeability evolution shows a monotonic, but decreasing trend (Fig. 10). The same cases (with the same micro- and meso-parameters) were solved for a bi-directional (0°/90°) two-layered structure, the only difference being the local permeability tensor of a yarn that contained also an axial component $k_{||}$ co-oriented with macro-flow. Obtained values of the macro-permeability are plotted in Fig. 10 as well. They are slightly higher than the ones of the unidirectional perpendicularly oriented structure, but show the same monotonic decreasing trend (Fig. 10). It can be observed that a very small change (of several microns) in the fibrous structure even at micro-scale – the inter-fiber distance – can generate under condition of fixed global fiber volume fraction a significant change in the macro-permeability of the structure, up to the order of magnitude. This confirms the importance of accounting for the microstructural parameters as well in the design of fibrous reinforcement with enhanced permeability, as it is done in this study.

When the flow is guided mostly by the meso-channels rather than by the micro-channels, the main flow tortuosity is significant, which means that the system dissipates more power due to the flow tortuosity. However, the corresponding global permeability is higher, regardless of the additional dissipation of energy caused by the tortuosity. This leads to the conclusion that the ratio of scales separation $k_\perp/h^2$ has a more significant effect on the global permeability of fibrous structure with fixed fiber volume fraction, than the flow tortuosity in the considered two-layered structure.

Quantitatively, in order to increase the macroscopic permeability, if a type of yarn with certain local permeability is selected, a distance h between them within the structure should be chosen as h_{min} from the condition $k_\perp/h^2 < 10^{-3}$, which ensures the inter-yarn flow to be dominant. It should be noted here that under these circumstances h implies the width of meso-channels that have the same orientation

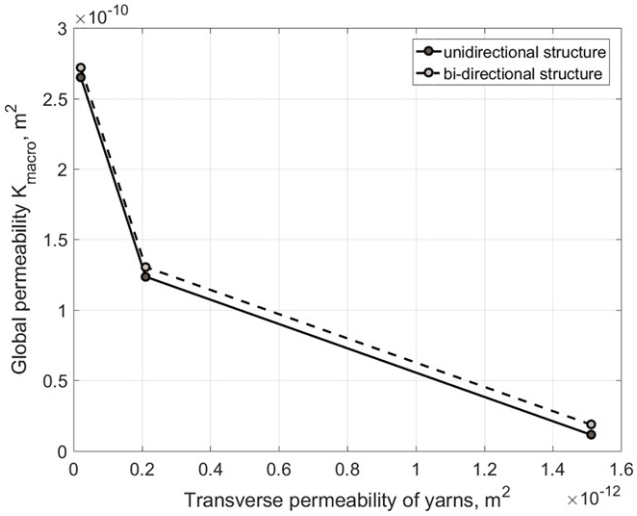

Fig. 10. Decrease of the global permeability with the increase of the local permeability of yarns for unidirectional and 0°/90° structure: global fiber volume fraction fixed ($V_{f_{total}} = 48\%$), fiber radius $r = 11\mu m$.

as the macroscopic pressure gradient of the in-plane flow system. This point will be considered in more details in the following section.

3.3. Influence of parameters of spatial configuration

Since the global fiber volume fraction of the structure being optimized is fixed, both parameters $k_\perp$ and h in the non-dimensional criterion $k_\perp/h^2$ mutually change: if $k_\perp$ increases, the inter-yarn pores h consequently reduces, and vice versa. It has been shown that in this case the meso-scale parameter h impacts more the macro-scale global permeability, than $k_\perp$. Besides, it has been shown for in-plane flow that this non-dimensional ratio of scales separation is a dominant parameter in the definition of the global permeability, compared to the flow tortuosity. This result was obtained in the considered preliminary simple configuration (Fig. 8b), where the flow tortuosity depends directly on the ratio $k_\perp/h^2 \gtrsim 10^{-3}$. In this case the global permeability of the structure was higher for lower permeability of yarns. The main flow surrounds the yarns, and, consequently, the global permeability was higher for higher tortuosity.

Furthermore, the effect of geometry is analyzed with the help of more complex configurations of yarns arrangement illustrated in Fig. 11 and the fixed ratio $k_\perp/h^2 = 1.1{\cdot}10^{-3}$ (equivalent to the case with inter-fiber distance of 5.5 μm of the configuration with 2 plies in Section 3.2). This value of the ratio $> 10^{-3}$ implies that when the fluid flows through the left-hand yarns, the flow tortuosity is reduced (Fig. 12). Though the flow tortuosity is much more significant in the zone around the right-hand yarn, for which the ratio is $< 10^{-3}$. The flow at the micro-scale is negligible in all simulated cases in this zone, as can be seen with the streamlines in Fig. 12, even if the mesoscopic distance d between the yarns varies (Fig. 11). Here we emphasize again the point that the parameter h in the non-dimensional ratio of scales separation defines the width of the channels that are collinear with the macroscopic pressure gradient of the in-plane flow system. When the width of the vertical channels is changed, the non-dimensional ratio for each of the yarns remains fixed, which allows to estimate independently the effect of tortuosity.

The flow in different configurations has also been calculated by the PGD method for all prescribed distances d after the parameterization of the domain geometry by the additional coordinate.

The local tortuosity decreases with the increase of distance d between the yarns. Even if the width d of vertical channels is very small compared to other channels, the main flow surrounds the yarns in this case, and is guided by the horizontal channels, instead of penetrating the yarn. This situation corresponds to the highest tortuosity. The decrease of the power dissipated by the flow can be observed with the decrease of the tortuosity, i.e. with the growth of the distance d between yarns (Fig. 13).

By complicating step by step the fibrous configurations, it was possible to study separately the effects of each of the parameters of interest on the global permeability of the structure, or on the dissipated power in the system. The presented estimation confirms that the effect of the ratio $k_\perp/h^2$ is dominant in comparison to the effect of in-plane flow tortuosity on the definition of mode of the flow (single-scale/multi-scale) through the fibrous reinforcement.

The following investigates if the flow modes, and thus the local tortuosity that impacts the global permeability, are defined by the same quantities in the case of through-thickness flow within the fibrous structure. For this purpose, a unidirectional configuration of 2 plies is considered (Fig. 14). The selected elementary unit cell represents one layer of half-fragments of two yarns and second layer shifted of 3/10 of the yarn length in order to keep the generality of the problem since slight shifting of layers or nesting effect often occurs in fibrous materials. Thus a lower layer is represented by 1/5-yarn distant from 4/5-yarn at the same distance that the yarns of the upper layer. This distance in the considered problem implies a previously discussed parameter h because it defines the size of channels collinear with macro-direction of flow. The geometrical values attributed in the numerical cases were taken so as to correspond to the existing unidirectional fabrics with fibers of 8.5 μm radius, yarns of local fiber volume fraction of 0.646 and dimensions of 3.23×0.87 mm, yarn spacing h of 310 μm. With these input values the local permeability of transverse isotropy of yarns $k_\perp$ estimated by Gebart's relation [26] is thus equal to $2.45{\cdot}10^{-13}$ m^2, which means that $k_\perp/h^2 < 10^{-3}$ for the through-thickness flow in this configuration. In the first simulated case (Fig. 14), with inter-layer distance $d = 310$ μm equal to the inter-yarn spacing, the flow shows a single-scale character, as the criterion for the in-plane flow states. However, while performing the same parametric change as described for the in-plane flow in this section, i.e. decreasing the parameter d, we can observe a switch of the through-thickness flow to its multi-scale mode (Fig. 14). All the other parameters except the inter-layer gap d were fixed in the simulations.

The fact that the criterion $k_\perp/h^2 \gtrsim 10^{-3}$ is not suitable for the definition of the flow mode for the through-thickness flow can be explained by the flattening of tows. Their usual high aspect ratio induces high local tortuosity of meso-pores between yarns for the through-thickness flow, which becomes dominant over the ratio between the meso- and microscopic typical pore sizes $k_\perp/h^2$ from the case of in-plane flow. At some point, the meso-pore tortuosity becomes so high that instead of surrounding the yarns only by the meso-channels, the flow follows micro-channels less tortuous within the yarns, which became the path of least resistance (Fig. 14). A criterion for the definition of the local flow mode in through-thickness direction should therefore contain apart from $k_\perp$, the sizes of both inter-layer and inter-yarn channels, and the dimensions of yarns.

Flow cases illustrated in Fig. 14 correspond to the global fiber volume fractions of 50% and 56%. Consideration of different fibrous configurations at constant global fiber volume fractions can help

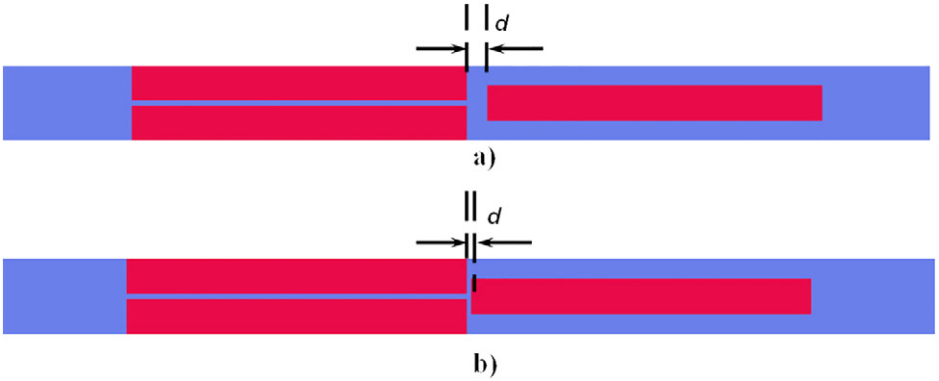

Fig. 11. Different geometrical configurations to introduce the in-plane flow tortuosity: yarn regions (in red) and inter-yarn pores (in blue).

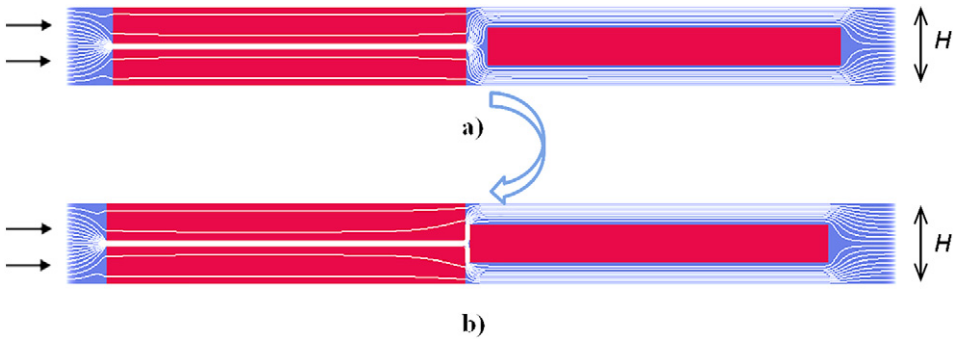

Fig. 12. Illustration of the tortuosity of streamlines, and the multi-scale and single-scale in-plane flow modes dependent on the inter-yarn gap d defined in Fig. 11: yarn regions (in red) and inter-yarn pores (in blue).

to reveal key parameters in the definition of enhanced through-thickness permeability. Let the yarn dimensions, as well as the yarn properties (V_f, $k_\perp$) stay fixed and the same as in the test-cases before. The influence of the inter-yarn spacing h and inter-layer gap d on the transverse permeability is analyzed in the sequel. Let the yarn spacing h take the values $h_1 = 310\ \mu m$ or $h_2 = 135\ \mu m$. The inter-layer gap d is varied so as to ensure different fiber volume fractions in their typical range. For the considered configuration (Fig. 14) the total V_f is related to other geometrical parameters via the expression:

$$V_{f_{total}} = V_{f_{yarn}} \cdot V_{f_{meso}} = V_{f_{yarn}} \cdot 2h_y l_y / ((2h_y + d) \cdot (l_y + h)) \tag{16}$$

where $V_{f_{yarn}}$ is the intra-yarn fiber volume fraction, $V_{f_{meso}}$ is the mesoscopic volume fraction of yarns in the structure, h_y and l_y are the yarn dimensions. The input geometrical parameters for transverse flow simulations are reported in Table 1.

The obtained through-thickness permeability values K_z with respect to different fixed global V_f are depicted in Fig. 15a. Thus fibrous configurations can be compared at fixed V_f in order to define those that are more favorable to the flow and have a higher permeability. Up to V_f around ≈56% the configuration with larger yarn spacing h_1 (compared to h_2) and smaller inter-layer gap d_1 has higher K_z. For higher V_f, due to the decrease of d_1, the meso-channels tortuosity becomes so significant that it decreases much more rapidly the permeability, and another configuration with smaller yarn spacing h_2 becomes the best configuration with enhanced permeability. Both configurations at $V_f = 56\%$ are depicted in Fig. 16, here $h_1 > h_2$, $d_1 < d_2$, $h_1 > d_1$ and $h_2 < d_2$. Therefore, by adjusting the inter-layer gap and inter-yarn spacing to meet the design requirements, it is possible to provide the fibrous structure with the same permeability K_z by different approaches.

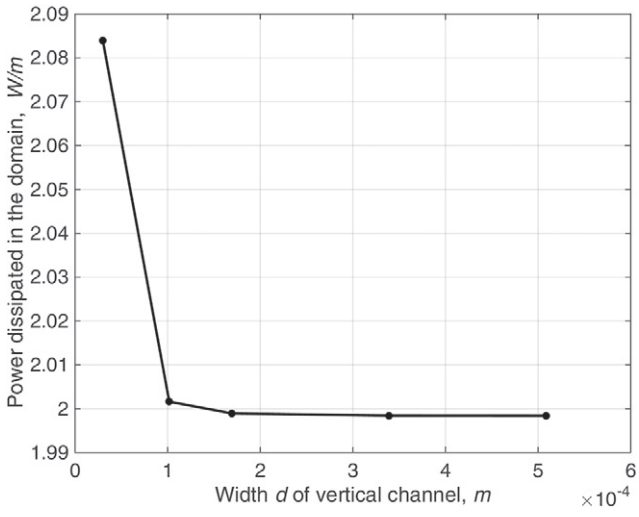

Fig. 13. Decrease of the power dissipated by the flow in the domain with decreasing effect of its tortuosity.

In the simulated cases it is observed that at lower V_f higher inter-yarn spacing (compared to the lower inter-yarn spacing and compared to the inter-layer gap) gives higher permeability. At high V_f the relation between the yarn spacings evolves in an inverse manner, but the yarn spacing of the second configuration with higher permeability at high V_f starts also to prevail over its inter-layer gap size. In order to estimate which geometrical effect on the permeability benefited from the intra-yarn flow, the problem was solved first with the Brinkman formulation, and for each of the calculated configurations the yarns were secondly assumed impermeable in order to solve the corresponding Stokes problem as well (Fig. 15). Thus it should be noted that in Fig. 15a the solutions of Stokes problem are plotted versus $V_{f_{total}}$ related to the corresponding Brinkman problem, but with real $V_{f_{total}}$ defined in Eq. (16) with $V_{f_{yarn}} = 1$ since the yarns are considered to be impermeable. This comparison indicates that the multi-scale character of the flow increases with $V_{f_{total}}$, and the intra-yarn flow starts to contribute more significantly to the macro-permeability value definition. The relative error between the permeability obtained from the solution of Brinkman equation and from the Stokes equation with neglected intra-yarn transverse flow $|K_{zBrinkman} - K_{zStokes}|/K_{zBrinkman} \cdot 100\%$ is shown in Fig. 15b. It quantifies the importance of multi-scale effects. For instance, starting from $V_f = 53\%$ for the first configuration with $h_1 = 310\mu m$, we obtain more than 1% of relative error. For the second configuration with $h_2 = 135\mu m$, the relative error for the whole range of the considered V_f is more than 1%. It is interesting to note that the curves for the definition of optimal permeability in Fig. 15a intersect at approximately the same value of V_f, at which the relative error between Stokes/Brinkman solutions for the first configuration with h_1 becomes higher.

In short, for the in-plane flow through fibrous reinforcements the main role in the definition of in-plane permeability of the structure is played by the size of the inter-layer gap, rather than the inter-yarn spacing, which can thus be reduced to the limit to improve the mechanical performance. Unlike the in-plane flow, the multi-scale character of the through-thickness flow is determined not only by the size of the channels aligned with the macro-flow, i.e. in this case the inter-yarn spacing within the same layer, but also by the size of the inter-layer gap and the yarn aspect ratio. Indeed, since fiber tows are usually flattened, they can create significant tortuous flow paths in the through-thickness flow. Further study is necessary to quantitatively establish a criterion as for the in-plane flow (Section 3.1) to discriminate between single-scale and multi-scale flow for the through-thickness flow through dual-scale porosity fibrous reinforcements.

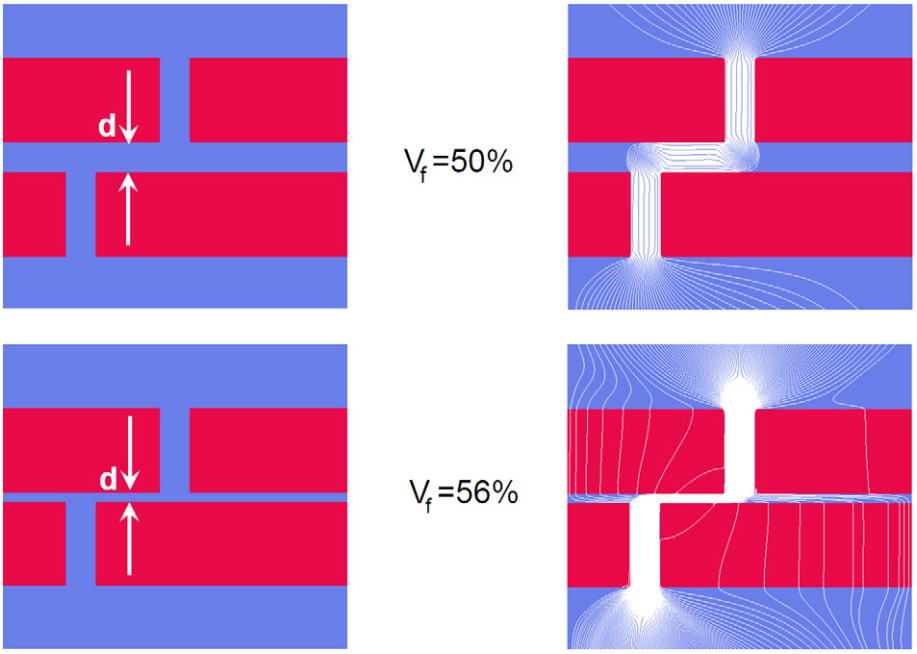

Fig. 14. Different modes of through-thickness flow in fibrous structure with the fixed ratio $k_\perp/h^2 < 10^{-3}$ and varying inter-layer gap d (and thus the global V_f).

4. Design of fibrous reinforcements with enhanced permeability

Following the guidelines established through the previous numerical study, the design of fibrous reinforcement with enhanced permeability is illustrated in this section on the wind energy sector. Its objective is to make longer rotor blades for the wind turbine, where the composite manufacturing process combined with the fibrous reinforcement are intended to provide stiffer nearly-flat components. Therefore, the heavyweight non-crimp fabrics (NCF) with high fiber volume fraction to ensure good mechanical performance and, at the same time enhanced axial in-plane and transverse permeabilities for the manufacturing by Liquid Resin Infusion (LRI) are regarded as an optimal solution. A suitable textile technology is needed to create and control the textile geometry of the double-scale fibrous material. Basically both the inter-tow and inter-layer gaps must be controlled while keeping the global fiber volume fraction fixed. This can be achieved using warp-knitted non-crimp fabric technology in combination with a specific design to obtain a satisfactory reproducibility [27].

The quasi-unidirectional non-crimp fabrics (quasi-UD NCF) presented in this study are manufactured from batches of Advantex glass roving (Owens-Corning). The quasi-UD NCF ply (Fig. 17) of total glass areal weight of 1395 g/m^2 is made of one layer of UD glass tows of 1335 g/m^2 areal weight (lineal density of 4800 *tex*) and one weft backing glass layer of 60 g/m^2 areal weight at $\pm 80^\circ$ orientation. Both layers are stitched with a very thin polyester thread. The $\pm 80^\circ$ weft backing layer brings stability to the fabric by offering support to the 0° UD tows and create the inter-layer gaps.

The influence of the inter-tow and inter-layer gaps on permeability is highlighted by comparing a reference (*REF*) quasi-UD NCF to enhanced permeability fabrics, that are in accordance with the principles deduced from the numerical study. The *REF* fabric is an NCF with a 5 *mm* stitch spacing and 68 *tex* roving for the $\pm 80^\circ$ weft yarns. The fabric designated as a fabric *A* (to keep the notation used in [28]) is designed with the doubled stitch density compared to the *REF* fabric: its spacing is 2.5 *mm*. This leads to a rise of the UD tow fiber volume fraction from 58% to 63% (see Table 2 with measured intra-yarn V_f), and provides more room between UD tows since the global fiber volume fraction is the same. An increase of the stitch density is meant to maintain open flow channels between yarns for the same level of compaction, typically a maximum of one atmosphere (0.1 *MPa*) in the LRI process. Therefore, the permeability measurements showed higher values of in-plane axial permeability K_x of the NCF *A* compared to the *REF* fabric [28] (Fig. 18), and hence following the trend explained in Section 3.2 and illustrated in Fig. 10.

Higher pre-compaction of tows in fabric *A* obtained by the denser stitching pattern makes this material less compliant at the typical low compaction force in LRI. This allows to keep inter-tow gaps more opened to flow and limits the bending of UD tows into the weft backing layer that are obstacles for the in-plane flow.

The fabric *C* (following the notation in [28]) differs from the *REF* fabric only by the increased lineal density of weft yarns to 200 *tex*, compared to 68 *tex* of the *REF*, while keeping a constant areal weight of the weft layer. Thus the weft backing layer exhibits a structure with bigger cells compared to the *REF* fabric (Fig. 19). Such design of fabric *C* allows to enhance the through-thickness permeability of

Table 1
Geometrical parameters used to study the through-thickness flow configurations.

Global V_f	0.5	0.51	0.52	0.53	0.54	0.55	0.56	0.57	0.58	0.59	0.6
Inter-layer gap d_1, μm	311	271	232	195	159	125	91	59	28		
Inter-yarn spacing h_1,μm	$h_1 = 310 \mu m$										
Inter-layer gap d_2,μm	418	376	335	296	258	222	187	153	120	89	58
Inter-yarn spacing h_2,μm	$h_2 = 135 \mu m$										
Yarn dimensions, *mm*	3.23×0.87										
Yarn parameters	$V_{fyarn} = 0.646$, $k_\perp = 2.45 \cdot 10^{-13}\ m^2$										

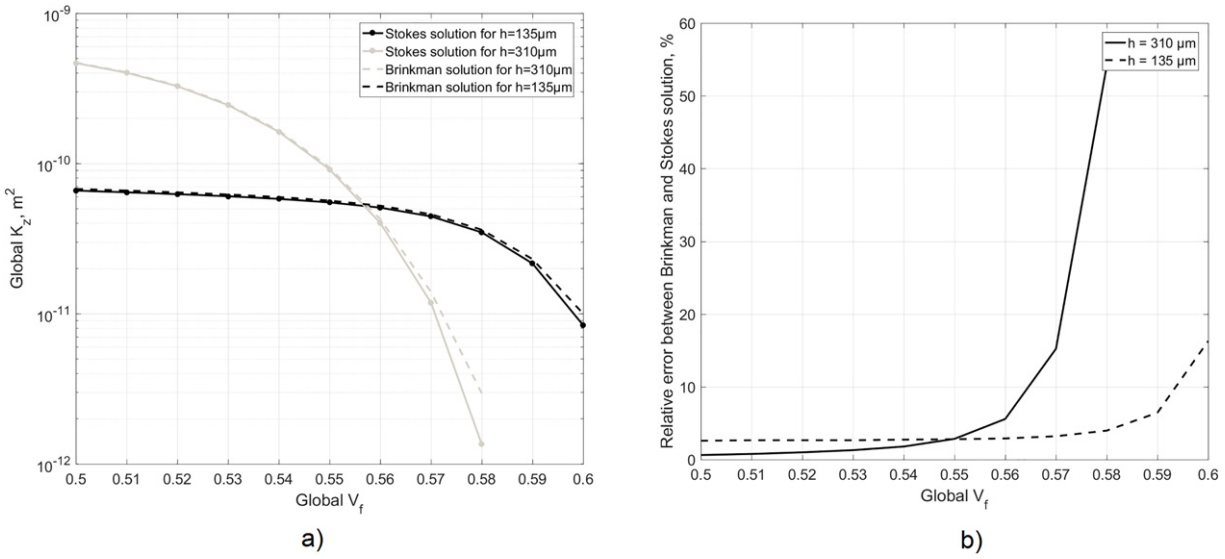

Fig. 15. a) Global K_z permeabilities of different geometrical configurations compared at fixed $V_{f_{total}}$ (defined in Eq. (16)) and obtained from the solution of Brinkman or Stokes equation; b) relative error between the K_z obtained from the solution of Brinkman and corresponding Stokes equations.

quasi-UD NCF, according to the principle discussed in Section 3.3. Indeed, the permeability measurements from [28] showed that especially for global fiber volume fraction higher than 52% the through-thickness permeability K_z of fabric *C* drops less quickly than the one of the *REF* fabric (Fig. 20). As shown in the previous section, an increase of V_f enables a multi-scale flow, which means that instead of flowing primarily around the yarns in the in-plane direction, the flow gradually takes the direct path in the through-thickness direction across the yarns. This is also supported by the fact that the in-plane permeability of fabric *C* is smaller than the one of the *REF* fabric, as reported in [28]. Therefore, since the flow across the yarns becomes significant at high V_f, the weft layer of fabric *C* with big cells provides easier connection in the thickness direction between the warp layers, it acts like a distribution medium to ease the impregnation of fibrous reinforcements. Big cells of the weft layer of fabric *C* represent the channels of characteristic dimension *h* in the previous numerical study, aligned with the macro-flow direction. They are bigger compared to the one in the *REF* fabric, while the inter-layer gap *d* is the same for both fibrous structures. One can infer from the analysis of the previous section that such a configuration with bigger *h*, same *d* and same global V_f gives higher through-thickness permeability, which is the case for the design of fabric *C*.

5. Conclusions

In order to design fibrous reinforcements with the objective to improve their impregnation by resin during the LCM processes, the multi-scale architecture of reinforcements was taken into account in this study by the use of the Brinkman equation, and with the access to the microscopic parameters at the scale of fibers as well via the analytic relations for the local permeability of yarns. This importance of modeling the fully multi-scale flow was confirmed by the demonstration that the sensitivity of the macro-permeability to a slight change in micro-scale fibrous architecture is significant: it can vary by an order of magnitude. Local velocity fields were numerically calculated by the Proper Generalized Decomposition method, and then a potential enhancement of the flow through the improved fibrous structure was evaluated by estimating the power dissipated by the flow through the reinforcement that was aimed to be minimized. In order to provide an enhanced permeability for the reinforcement, but not at the cost of the reduced mechanical performance of a final composite part, the design study was carried out under the condition of constant total fiber volume fraction.

With the aim of increasing the global permeability of the reinforcement the influence of the following parameters was analyzed:

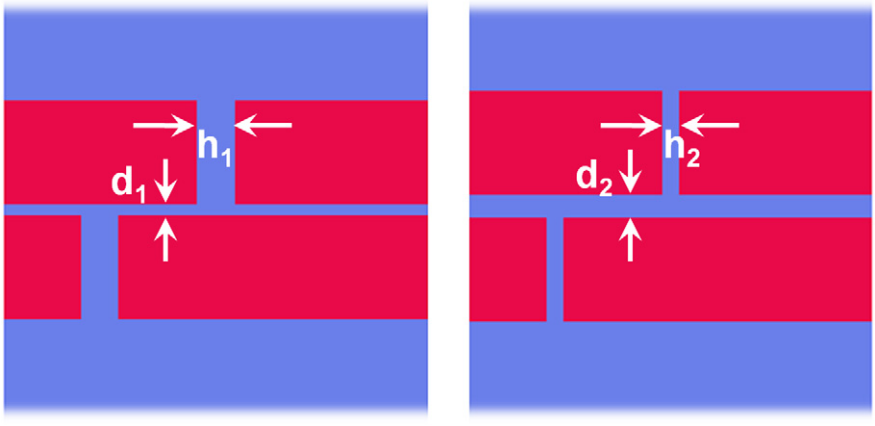

Fig. 16. Geometrical configurations with the same yarn dimensions, global $V_f = 56\%$ and leading to equal through-thickness permeabilities K_z.

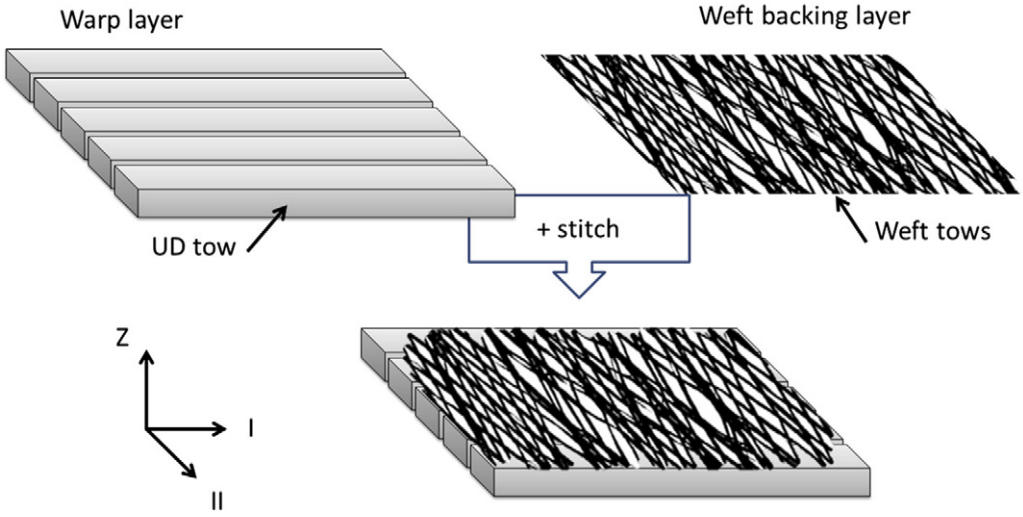

Fig. 17. 3D representation of quasi-UD NCF fabric [28].

the distribution of sizes of mesoscopic inter-yarn pores and microscopic intra-yarn pores, as well as the inter-yarn topology that mainly impacts the flow tortuosity. The model reduction method allowed to efficiently conduct a parametric study, in which the separated representation of the sought solution included additionally the functions dependent on geometrical parameters of the problem. Consequently, the problem could be solved for a large range of parameters values at once, what is advantageous compared to series of classical calculations for different combinations of parameters.

The parametric study allowed to define a criterion for the evaluation of mutual relation between the in-plane micro-scale flow (inside the yarns) and meso-scale flow (between the yarns). It indicates in which cases the in-plane flow through the fibrous reinforcement degenerates into a single-scale flow where the intra-tow flow can be neglected. This criterion relates the micro- and mesoscopic typical problem dimensions within the ratio k/h^2, where k is the micro-scale permeability of yarns and h is the inter-layer pores size. It was concluded that the inter-yarn spacing within the same layer is not an important parameter for the in-plane flow, which is not the case for the through-thickness flow through fibrous structure. The multi-/single-scale nature of the flow in the thickness direction is determined simultaneously by the size of the inter-layer gap, inter-yarn spacing, yarns aspect ratio, and their local permeability, and further study is necessary for its criterion definition. It was shown that with the increasing global V_f the microscopic intra-yarn flow gains more and more importance in the definition of the macro-permeability both for the in-plane and through-thickness direction. It gives a particular contribution in the case of the through-thickness flow since the local flow changes from the primarily in-plane mode (progressing around flat yarns) to the direct through-thickness path.

Under condition of constant global fiber volume fraction for the in-plane flow it was shown for unidirectional and bidirectional reinforcements that even with the increase of the local intra-yarn permeability, the global in-plane permeability of the structure can decrease. It means that in the ratio of scale separation k/h^2 the role of mesoscopic inter-layer gaps h is dominant compared to the microscopic pores. Increase of the global permeability, or decrease of the power dissipated in the system, with the increase of scale separation is monotonic, there is no optimum. Besides, the effect of the scale separation k/h^2 in the in-plane flow was shown to dominate the effect of main flow tortuosity. Even if a stronger scale separation results in higher tortuosity, when the main flow gets around the yarns and does not flow inside, it increases the macro-permeability. However, for the through-thickness flow where the meso-pores between the high-aspect-ratio yarns force the fluid to follow very tortuous paths, the main flow tortuosity becomes a non-negligible parameter. Reinforcements whose meso-pore structure does not involve too much tortuosity as V_f increases will have higher transverse macro-permeability at high fiber volume fractions. At lower fiber volume fractions reinforcements with larger inter-yarn spacing, even if their inter-layer gap is smaller, have higher through-thickness permeability because this parameter prevails at low V_f. Principles established through the numerical analysis of this study allow to design fibrous reinforcements with enhanced permeability. They were applied to the quasi-unidirectional warp-knitted non-crimp fabric with the controlled inter-yarn and inter-layer gaps for the fixed global fiber volume fraction.

As a perspective, the design of multi-scale fibrous reinforcements at fixed fiber volume fraction can also consider the transient flow

Table 2
Average measured intra-yarn UD fiber volume fraction for each reinforcement.

	REF	*A*	*C*
$V_{f_{yarn}}$, %	58.3 (±4.2)	63.1 (±1.2)	64.6 (±1.5)

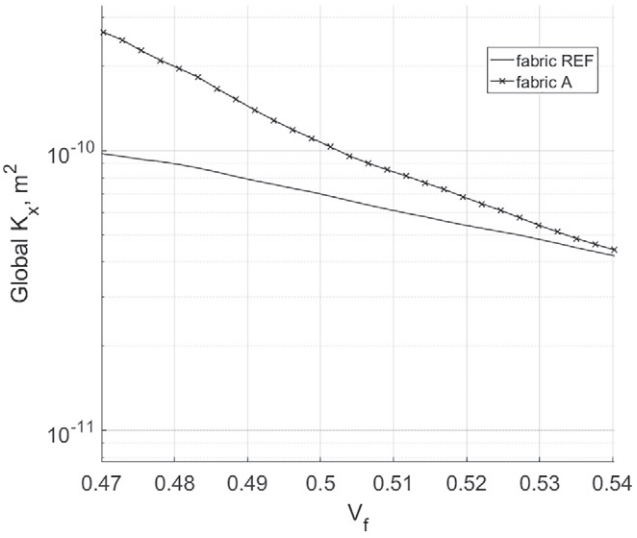

Fig. 18. Comparison of measured in-plane axial permeabilities K_x of quasi-UD NCF *REF* and *A* with respect to the global fiber volume fraction V_f [28].

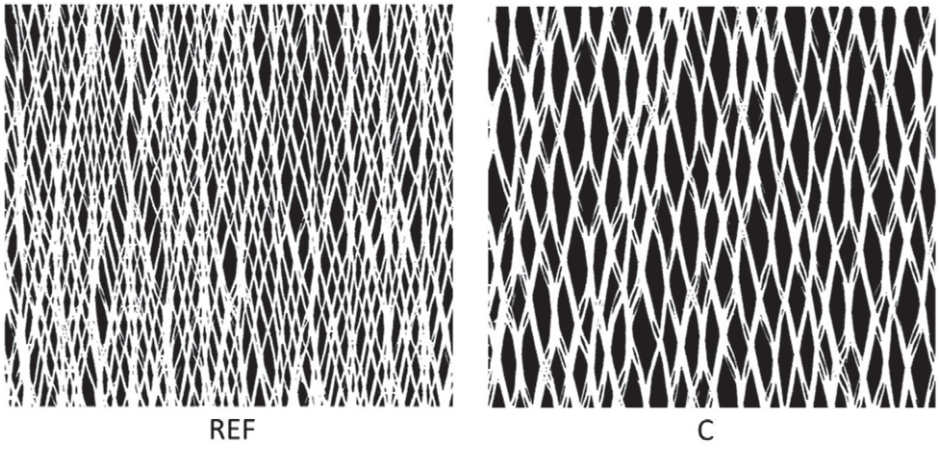

Fig. 19. Structure differences of the weft backing layer (reconstructed from images) of the *REF* fabric with 68 *tex* rovings and fabric *C* with 200 *tex* rovings [28].

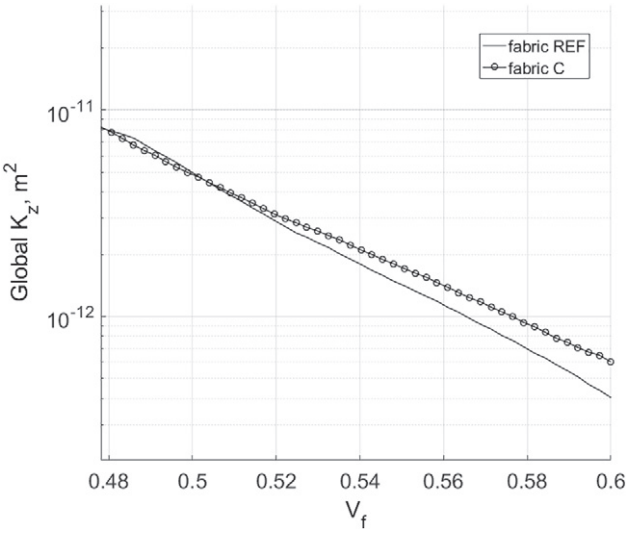

Fig. 20. Comparison of measured through-thickness permeabilities K_z of quasi-UD NCF *REF* and *C* with respect to the global fiber volume fraction V_f [28].

condition where the fluid/fiber wetting influences the impregnation at the front. The issue at the small scale is that when the tows are getting highly compacted, on the one hand, their local permeability decreases, and on the other hand, their wetting capability improves due to the capillarity. Thus it would be of interest to investigate how these mechanisms compete with each other.

Acknowledgments

The French ANR (Agence Nationale de la Recherche) is gratefully acknowledged for the financial support received through the collaborative project TAPAS-LCM (Nr. ANR-2011-RMNP-0020).

References

[1] M. Deleglise, P. Le Grognec, C. Binetruy, P. Krawczak, B. Claude, Modeling of high speed RTM injection with highly reactive resin with on-line mixing, Compos. A: Appl. Sci. Manuf. 42 (10) (2011) 1390–1397.
[2] N.R.L. Pearce, F.J. Guild, J. Summerscales, An investigation into the effects of fabric architecture on the processing and properties of fibre reinforced composites produced by resin transfer moulding, Compos. A: Appl. Sci. Manuf. 29 (1–2) (1998) 19–27.
[3] N.R.L. Pearce, J. Summerscales, F.J. Guild, Improving the resin transfer moulding process for fabric-reinforced composites by modification of the fabric architecture, Compos. A: Appl. Sci. Manuf. 31 (12) (2000) 1433–1441.
[4] H. Brinkman, A calculation of the viscous force exerted by a flowing fluid on a dense swarm of particles, Appl. Sci. Res. 1 (1) (1949) 27–34.
[5] C.L. Tucker, III, R.B. Dessenberger, Flow and rheology in polymer composites manufacturing, Governing equations for flow and heat transfer in stationary fiber beds, Elsevier Science Publishers. 1994, (chapter).
[6] J.A. Ochoa-Tapia, S. Whitaker, Momentum transfer at the boundary between a porous medium and a homogeneous fluid - I. Theoretical development, Int. J. Heat Mass Transf. 38 (14) (1995) 2635–2646.
[7] X. Zeng, L.P. Brown, A. Endruweit, M. Matveev, A.C. Long, Geometrical modelling of 3D woven reinforcements for polymer composites: prediction of fabric permeability and composite mechanical properties, Compos. A: Appl. Sci. Manuf. 56 (2014) 150–160.
[8] M. Chandesris, D. Jamet, Jump conditions and surface-excess quantities at a fluid/porous interface: a multi-scale approach, Transp. Porous Media 78 (3) (2009) 419–438.
[9] G.S. Beavers, D.D. Joseph, Boundary conditions at a naturally permeable wall, J. Fluid Mech. 30 (1) (1967) 197–207.
[10] M.A.A. Spaid, F.R. Phelan, Lattice Boltzmann methods for modeling microscale flow in fibrous porous media, Phys. Fluids 9 (9) (1997) 2468–2474.
[11] E.B. Belov, S.V. Lomov, I. Verpoest, T. Peters, D. Roose, R.S. Parnas, K. Hoes, H. Sol, Modelling of permeability of textile reinforcements: lattice Boltzmann method, Compos. Sci. Technol. 64 (7–8) (2004) 1069–1080.
[12] N.D. Ngo, K.K. Tamma, Microscale permeability predictions of porous fibrous media, Int. J. Heat Mass Transf. 44 (16) (2001) 3135–3145.
[13] E. Lopez, E. Abisset-Chavanne, F. Lebel, R. Upadhyay, S. Comas, C. Binetruy, F. Chinesta, Flow modeling of linear and nonlinear fluids in two and three scale fibrous fabrics, Int. J. Mater. Form. 9 (2) (2016) 215–227.
[14] B. Verleye, R. Croce, M. Griebel, M. Klitz, S.V. Lomov, G. Morren, H. Sol, I. Verpoest, D. Roose, Permeability of textile reinforcements: simulation, influence of shear and validation, Compos. Sci. Technol. 68 (13) (2008) 2804–2810.
[15] W.R. Hwang, S.G. Advani, Numerical simulations of Stokes-Brinkman equations for permeability prediction of dual scale fibrous porous media, Phys. Fluids 22 (11) (2010) 113101.
[16] H. Tan, K.M. Pillai, Finite element implementation of stress-jump and stress–continuity conditions at porous-medium, clear-fluid interface, Comput. Fluids 38 (6) (2009) 1118–1131.
[17] B. Yu, L.J. Lee, A simplified in-plane permeability model for textile fabrics, Polym. Compos. 21 (5) (2000) 660–685.
[18] Y.S. Song, J.R. Youn, Asymptotic expansion homogenization of permeability tensor for plain woven fabrics, Compos. A: Appl. Sci. Manuf. 37 (11) (2006) 2080–2087.
[19] F. Chinesta, A. Ammar, A. Leygue, R. Keunings, An overview of the proper generalized decomposition with applications in computational rheology, J. Non-Newtonian Fluid Mech. 166 (11) (2011) 578–592.
[20] A. Leygue, E. Verron, A first step towards the use of proper general decomposition method for structural optimization, Arch. Comput. Meth. Eng. 17 (4) (2010) 465–472.
[21] A.K. Al-Hadhrami, L. Elliott, D.B. Ingham, X. Wen, Fluid flows through two-dimensional channels of composite materials, Transp. Porous Media 45 (2) (2001) 281–300.
[22] J. Summerscales, P.R. Griffin, S.M. Grove, F.J. Guild, Quantitative microstructural examination of RTM fabrics designed for enhanced flow, Compos. Struct. 32 (1–4) (1995) 519–529.
[23] F. Chinesta, A. Leygue, F. Bordeu, J.V. Aguado, E. Cueto, D. Gonzalez, I. Alfaro, A. Ammar, A. Huerta, PGD-based computational vademecum for efficient design, optimization and control, Arch. Comput. Meth. Eng. 20 (1) (2013) 31–59.
[24] T. Heuzé, A. Leygue, G. Racineux, Parametric modeling of an electromagnetic compression device with the proper generalized decomposition, Int. J. Mater. Form. 9 (1) (2016) 101–113.

[25] E. Giner, B. Bognet, J.J. Ròdenas, A. Leygue, F.J. Fuenmayor, F. Chinesta, The Proper Generalized Decomposition (PGD) as a numerical procedure to solve 3D cracked plates in linear elastic fracture mechanics, Int. J. Solids Struct. 50 (10) (2013) 1710–1720.
[26] B.R. Gebart, Permeability of unidirectional reinforcements for RTM, J. Compos. Mater. 26 (8) (1992) 1100–1133.
[27] S.V. Lomov, Non-crimp fabric composites: manufacturing, properties and applications, Elsevier. 2011.
[28] B. Martin, S. Comas-Cardona, C. Binetruy, N. Billon, J. Bouvard, P. Lucas, Influence of fabrics' design parameters on the morphology and 3D permeability tensor of quasi-unidirectional non-crimp fabrics, Compos. A: Appl. Sci. Manuf. 90 (2016) 470–479.